Hindawi
Journal of Function Spaces
Volume 2017, Article ID 6910926, 13 pages
https://doi.org/10.1155/2017/6910926

Research Article

Rogue Wave Solutions and Generalized Darboux Transformation for an Inhomogeneous Fifth-Order Nonlinear Schrödinger Equation

N. Song,[1] W. Zhang,[2] P. Wang,[1] and Y. K. Xue[1]

[1]*Department of Mathematics, North University of China, Taiyuan, Shanxi 030051, China*
[2]*College of Mechanical Engineering, Beijing University of Technology, Beijing 100022, China*

Correspondence should be addressed to Y. K. Xue; xyk5152@163.com

Received 25 March 2017; Accepted 2 May 2017; Published 27 August 2017

Academic Editor: Hua Su

The rogue wave solutions are discussed for an inhomogeneous fifth-order nonlinear Schrödinger equation, which describes the dynamics of a site-dependent Heisenberg ferromagnetic spin chain. Using the Darboux matrix, the generalized Darboux transformation is constructed and a recursive formula is derived. Based on the transformation, the first-order to the third-order rogue wave solutions are obtained. Then, the nonlinear dynamics of the first-order to the third-order rogue waves are studied on the basis of some free parameters. Several new structures of the rogue waves are found using numerical simulation. The conclusions will be a supportive tool to study the rogue waves better.

1. Introduction

For some decades, some researchers have focused on the rogue waves which were firstly used by Draper [1]. Rogue waves are also called killer waves, freak waves, giant waves, monster waves, or extreme waves, which appeared in nautical mythology, entered the ocean waves [2–4], and gradually moved into other fields, such as optics [5–7], matter waves [8], superfluids [9], plasmas [10], atmosphere [11], and even finance [12]. The common characteristics and differences in various fields of physics are under discussion [13]. The phenomenon of the rogue waves is not fully understood up to now. Therefore, continuous studies on the rogue waves will enrich the concept and bring a full understanding of the mysterious phenomenon.

The first model describing the rogue waves was the focusing nonlinear Schrödinger (NLS) equation

$$iq_t + \frac{1}{2}q_{xx} + |q|^2 q = 0, \tag{1}$$

which is an integrable system and plays an important role in the study of the rogue waves. As is well known, there are many research results on the rogue waves of (1). The first-order rational solution was derived by Peregrine [14] and the second-order one was obtained using the modified Darboux transformation (DT) [15]. The DT is an effective tool for constructing the solution of the integrable systems [16], which came from the work of Darboux on the Sturm-Liouville equation. Recently, the generalized DT [17] was proposed, which is a new and simpler method to construct the higher-order rational solution of the rogue waves of (1). By making use of the generalized DT, Zhaqilao [18] investigated the first-order and the second-order solutions of the rogue waves for the generalized nonlinear Schrödinger equation, Song et al. [19] obtained the higher-order solutions of the rogue waves for the fourth-order dispersive nonlinear Schrödinger equation, and Lv and Lin [20] solved the three coupled higher-order nonlinear Schrödinger equations with the achievement of n-soliton formula and derived the lump solutions [21].

Nonlinear phenomena can be described mathematically on the basis of the corresponding nonlinear evolution equations, through which we can study the potential nonlinear dynamics. The Heisenberg models of ferromagnetics with

different magnetic interactions in the semiclassical and continuum limits are considered as a class of the nonlinear evolution equations and had a connection with nonlinear spin excitations and the nonlinear Schrödinger equation [22, 23]. In the Heisenberg ferromagnetism, the nonlinear Schrödinger equation is used to describe the dynamics of nonlinear spin excitation [24]. When the ferromagnetic spin chain is site-dependent, the nonlinear Schrödinger equation is modified as the inhomogeneous nonlinear Schrödinger one [25].

In the paper, we will consider an inhomogeneous fifth-order nonlinear Schrödinger equation as follows [26, 27]:

$$\begin{aligned} & iq_t - i\varepsilon q_{xxxxx} - 10i\varepsilon q_{xxx} - 20i\varepsilon q_x q^* q_{xx} - 30i\varepsilon |q|^4 q_x \\ & - 10i\varepsilon \left(|q_x|^2 q\right)_x + (fq)_{xx} \\ & + 2q\left[f|q|^2 + \int_{-\infty}^{x} f_{x'}\left(x'\right)\left|q\left(x',t\right)\right|^2 \mathrm{d}x'\right] \\ & - i(gq)_x = 0, \end{aligned} \tag{2}$$

where $q(x,t)$ is a complex function and t and x denote the scaled time and spatial coordinate, respectively. f and g represent the variation of the bilinear and biquadratic exchange interactions at different sites along the spin chain and

$$\begin{aligned} f &= f_1 x + f_2, \\ g &= g_1 x + g_2, \end{aligned} \tag{3}$$

where f_j and g_j $(j = 1, 2)$ are real constants. ε is a perturbation parameter and the asterisk is the complex conjugation.

Equation (2) is generated from the deformation of the inhomogeneous Heisenberg ferromagnetic system with the prolongation structure, which describes the dynamics of a site-dependent Heisenberg ferromagnetic spin chain [28]. It is an integrable nonlinear equation. Wang et al. [26] constructed the Darboux transformation and represented one- and two-soliton solutions of (2).

For the second-order to fourth-order nonlinear Schrödinger equations, a lot of research has been done, including the rogue waves [18, 19], soliton solutions [29–31], modulation instability, integrability [32–34], and rational solutions [35]. However, to the best of our knowledge, the rogue wave solution for the fifth-order nonlinear Schrödinger equation has never been reported in the literature.

The paper is to obtain Nth-order rogue waves solutions for the inhomogeneous fifth-order nonlinear Schrödinger equation using the generalized DT. On the basis of the DT matrix, the generalized DT is constructed and the formula is derived which will generate Nth-order solution of the rogue waves. The nonlinear dynamics of the first-order to the third-order rogue waves are discussed with the influence of some parameters and the interesting structures are showed.

2. Generalized Darboux Transformation

The Lax pair will ensure the integrability of the nonlinear equations, which is effective in constructing the solutions by using the Darboux transformation. The Lax pair is given as follows [26]:

$$\Phi_x = U\Phi = \left(\lambda U_0 + U_1\right)\Phi, \tag{4a}$$

$$\Phi_t = V\Phi = \begin{pmatrix} A & B \\ -B^* & -A \end{pmatrix}\Phi, \tag{4b}$$

where U and V are 2×2 matrices

$$\begin{aligned} U_0 &= -i\begin{pmatrix} 1 & 0 \\ 0 & -1 \end{pmatrix}, \\ U_1 &= \begin{pmatrix} 0 & q \\ -q^* & 0 \end{pmatrix}, \\ A &= -16i\lambda^5\varepsilon + 8i\lambda^3\varepsilon|q|^2 + 4\lambda^2\varepsilon\left(qq_x^* - q_x q^*\right) - 2if\lambda^2 \\ & - 2i\lambda\varepsilon\left(qq_{xx}^* + q^* q_{xx} - |q_x|^2 + 3|q|^4\right) - ih\lambda \\ & + \varepsilon\left(q^* q_{xxx} - qq_{xxx}^* + q_x q_{xx}^* - q_{xx}q_x^* + 6|q|^2 q^* q_x\right. \\ & \left. - 6|q|^2 q_x^* q\right) + if|q|^2 + i\left[f|q|^2\right. \\ & \left. + \int_{-\infty}^{x} f_{x'}\left(x'\right)\left|q\left(x',t\right)\right|^2 \mathrm{d}x'\right], \\ B &= 16\lambda^4\varepsilon q + 8i\lambda^3\varepsilon q_x - 4\lambda^2\varepsilon\left(q_{xx} + 2|q|^2 q\right) \\ & - 2i\lambda\varepsilon\left(q_{xxx} + 6|q|^2 q_x\right) + 2f\lambda q + \varepsilon\left(q_{xxxx}\right. \\ & \left. + 8|q|^2 q_{xx} + 2q^2 q_{xx}^* + 4|q_x|^2 q + 6q_x^2 q^* + 6|q|^4 q\right) \\ & + i(fq)_x + hq, \end{aligned} \tag{5}$$

where $\Phi = (\varphi, \phi)^{\mathrm{T}}$ is an eigenfunction of the Lax pair (4a) and (4b), q is a potential function, λ is a constant spectral parameter, and the asterisk denotes complex conjugate.

Using the Maple, (2) can be deduced from the compatibility condition, namely, the zero-curvature equation

$$U_t - V_x + [U, V] = 0. \tag{6}$$

The Darboux transformation consists of the eigenfunction transformation and potential transformation, which is a gauge transformation

$$\Phi[1] = T\Phi \tag{7}$$

of the solution for the Lax pair (4a) and (4b). T is a Darboux matrix, which will transform the Lax pair (4a) and (4b) into a new one; that is to say,

$$\begin{aligned} \Phi[1]_x &= U^{[1]}\Phi[1], \\ \Phi[1]_t &= V^{[1]}\Phi[1]. \end{aligned} \tag{8}$$

It is known that $U^{[1]}$ and $V^{[1]}$ have the same form as U and V when q and q^* in the matrices U and V are substituted by $q[1]$ and $q[1]^*$ in the matrices $U^{[1]}$ and $V^{[1]}$. $U^{[1]}$ and $V^{[1]}$ are given by

$$\begin{aligned} U^{[1]} &= \left(T_x + TU\right) T^{-1}, \\ V^{[1]} &= \left(T_t + TV\right) T^{-1}. \end{aligned} \tag{9}$$

According to (9), a relationship between the new potential function $q[1]$ and the initial potential function q will be established. Thus, the Darboux matrix T is defined as [16]

$$T = \lambda I - S, \quad S = H\Lambda H^{-1}, \tag{10}$$

where

$$\begin{aligned} I &= \begin{pmatrix} 1 & 0 \\ 0 & 1 \end{pmatrix}, \\ H &= \begin{pmatrix} \varphi_1 & \phi_1^* \\ \phi_1 & -\varphi_1^* \end{pmatrix}, \\ \Lambda &= \begin{pmatrix} \lambda_1 & 0 \\ 0 & \lambda_1^* \end{pmatrix}. \end{aligned} \tag{11}$$

Let $\Phi_1 = (\varphi_1, \phi_1)^{\mathrm{T}}$ be an eigenfunction of the Lax pair (4a) and (4b) with a seeding solution $q = q[0]$ and $\lambda = \lambda_1$. It is seen that $(\phi_1^*, -\varphi_1^*)^{\mathrm{T}}$ can also satisfy equation (4a) and (4b) with $\lambda = \lambda_1^*$. Selecting different eigenfunctions $\Phi_k = (\varphi_k, \phi_k)^{\mathrm{T}}$ at λ_k, respectively, the above Darboux transformation procedure can be easily iterated.

Therefore, on the basis of the Darboux matrix T in (9), the initial Darboux transformation of equation (2) is given as

$$\begin{aligned} \Phi_1[0] &= T[0]\Phi_1, \\ q[1] &= q[0] - 2i\left(\lambda_1 - \lambda_1^*\right) \frac{\varphi_1[0]\phi_1^*[0]}{\left|\varphi_1[0]\right|^2 + \left|\phi_1[0]\right|^2}, \end{aligned} \tag{12}$$

where

$$T[1] = \lambda_2 I - H[0]\Lambda[1]H[0]^{-1}, \tag{13a}$$

$$\begin{aligned} T[0] &= I, \\ H[0] &= \begin{pmatrix} \varphi_1[0] & \phi_1^*[0] \\ \phi_1[0] & -\varphi_1^*[0] \end{pmatrix}, \\ \Lambda[1] &= \begin{pmatrix} \lambda_1 & 0 \\ 0 & \lambda_1^* \end{pmatrix}, \\ \Phi_1[0] &= \left(\varphi_1[0], \phi_1[0]\right)^{\mathrm{T}} = \left(\varphi_1, \phi_1\right)^{\mathrm{T}} = \Phi_1, \\ q[0] &= q. \end{aligned} \tag{13b, 13c}$$

If N different basic solutions $\Phi_k = (\varphi_k, \phi_k)^{\mathrm{T}}$ $(k = 1, 2, \ldots, N)$ of the Lax pair (4a) and (4b) at $\lambda = \lambda_k$ $(k = 1, 2, \ldots, N)$ are given, the initial Darboux transformation can be iterated N times. Then the Nth-step DT for (2) is

$$\begin{aligned} &\Phi_N[N-1] \\ &\quad = T[N-1]T[N-2]\cdots T[1]T[0]\Phi_N, \end{aligned} \tag{14a}$$

$$\begin{aligned} &q[N] \\ &\quad = q[0] \\ &\qquad - 2i\sum_{k=1}^{N}\left(\lambda_1 - \lambda_1^*\right)\frac{\varphi_k[k-1]\phi_k^*[k-1]}{\left|\varphi_k[k-1]\right|^2 + \left|\phi_k[k-1]\right|^2}, \end{aligned} \tag{14b}$$

where

$$T[k] = \lambda_{k+1} I - H[k-1]\Lambda[k]H[k-1]^{-1}, \tag{15a}$$

$$\begin{aligned} H[k-1] &= \begin{pmatrix} \varphi_k[k-1] & \phi_k^*[k-1] \\ \phi_k[k-1] & -\varphi_k^*[k-1] \end{pmatrix}, \\ \Lambda[k] &= \begin{pmatrix} \lambda_k & 0 \\ 0 & \lambda_k^* \end{pmatrix}, \end{aligned} \tag{15b}$$

$$\begin{aligned} &\Phi_k[k-1] \\ &\quad = \left(T[k-1]T[k-2]\cdots T[1]T[0]\right)|_{\lambda=\lambda_k}\Phi_k, \\ &\qquad (k = 1, 2, \ldots, N). \end{aligned} \tag{15c}$$

The initial value is $\Phi_1[0] = (\varphi_1[0], \phi_1[0])^{\mathrm{T}} = (\varphi_1, \phi_1)^{\mathrm{T}} = \Phi_1$.

On the basis of the former elementary DT, a generalized DT is derived for (2). We assume that

$$\Psi = \Phi_1\left(\lambda_1, \delta\right) \tag{16}$$

is a special solution of the Lax pair (4a) and (4b) and δ is a small parameter.

Using the Taylor series, Ψ can be expanded at $\delta = 0$

$$\Psi = \Phi_1^{[0]} + \Phi_1^{[1]}\delta + \Phi_1^{[2]}\delta^2 + \cdots + \Phi_1^{[m]}\delta^m + o\left(\delta^m\right), \tag{17}$$

where $\Phi_1^{[j]} = (1/j!)(\partial^j/\partial\lambda^j)\Phi_1(\lambda)|_{\lambda=\lambda_1}$ $(j = 1, 2, \ldots, m)$.

From the above assumption, it is easily seen that $\Phi_1^{[0]} = \Phi_1[0]$ is a particular solution of the Lax pair (4a) and (4b) with $q = q[0]$ and $\lambda = \lambda_1$. Therefore, an Nth-step generalized DT is constructed by combining all the Darboux matrices

$$\begin{aligned}
&\Phi_1[N-1] \\
&= \Phi_1^{[0]} + \left[\sum_{l=1}^{N-1} T_1[l]\right]\Phi_1^{[1]} \\
&\quad + \left[\sum_{l=1}^{N-1}\sum_{k>l}^{N-1} T_1[k]\,T_1[l]\right]\Phi_1^{[2]} + \cdots \\
&\quad + \left[T_1[N-1]\,T_1[N-2]\cdots T_1[1]\right]\Phi_1^{[N-1]}, \\
&q[N] \\
&= q[N-1] \\
&\quad - 2i\left(\lambda_1 - \lambda_1^*\right)\frac{\varphi_1[N-1]\,\phi_1[N-1]^*}{\left|\varphi_1[N-1]\right|^2 + \left|\phi_1[N-1]\right|^2},
\end{aligned} \tag{18}$$

where

$$T_1[k] = \lambda_1 I - H_1[k-1]\,\Lambda[1]\,H_1[k-1]^{-1}, \tag{19a}$$

$$H_1[k-1] = \begin{pmatrix} \varphi_k[k-1] & \phi_k^*[k-1] \\ \phi_k[k-1] & -\varphi_k^*[k-1] \end{pmatrix}, \tag{19b}$$

$$\Phi_1[k-1] = \begin{pmatrix} \varphi_k[k-1] \\ \phi_k[k-1] \end{pmatrix}, \quad (k = 1, 2, \ldots, N). \tag{19c}$$

Equations (18), (19a), (19b), and (19c) are the recursive formulae of the Nth-step generalized DT for (2), which are simple to construct the higher-order rogue waves solutions and can be transformed into the $2n \times 2n$ determinant representation making use of the Crum theorem [16]. On the basis of the rogue waves solutions of (2), the figures of the first- to the third-order rogue waves will be discussed in the next section.

3. Rogue Waves Solutions

In order to calculate easily, the rogue waves solutions are derived when the inhomogeneous parameters are independent of x; that is to say, $f_1 = g_1 = 0$. The parameters are chosen as $f_2 = 0.5$ and $g_2 = -25\varepsilon$.

It is known that the higher-order solutions of the rogue waves will be obtained with the seed solution and initial eigenfunction. To begin with, the seed solution is equal to $q[0] = e^{it}$. The corresponding eigenfunction $\Phi_1(\lambda)$ for the linear spectral problem at $\lambda = ih$ is

$$\Phi_1(\lambda) = \begin{pmatrix} \left(C_1 e^{A} + C_2 e^{-A}\right) e^{it/2} \\ \left(C_2 e^{A} + C_1 e^{-A}\right) e^{-it/2} \end{pmatrix}, \tag{20}$$

where

$$\begin{aligned}
C_1 &= \frac{\sqrt{h + \sqrt{h^2 - 1}}}{\sqrt{h^2 - 1}}, \\
C_2 &= -\frac{\sqrt{h - \sqrt{h^2 - 1}}}{\sqrt{h^2 - 1}}, \\
A &= \sqrt{h^2 - 1}\,(x + \omega t + \Omega(\delta)),
\end{aligned} \tag{21a}$$

$$\omega = 16(ih)^4\varepsilon - 8(ih)^2\varepsilon + 2f_2(ih) + 6\varepsilon + g_2, \tag{21b}$$

$$\Omega(\delta) = \sum_{j=1}^{n}\left(a_j + ib_j\right)\delta^{2j} \quad \left(a_j, b_j \in R\right), \tag{21c}$$

and δ is a small parameter and $\Omega(\delta)$ is the separating function, which contains $2n$ free parameters a_j, b_j ($j = 1, \ldots, n$) and a_j, b_j are real constants.

Let $h = 1 + \delta^2$ and expanding the vector function $\Phi_1(\delta)$ at $\delta = 0$, we have

$$\begin{aligned}
\Phi_1(\delta) &= \Phi_1^{[0]} + \Phi_1^{[1]}\delta^2 + \Phi_1^{[2]}\delta^4 + \cdots + \Phi_1^{[m]}\delta^{2m} \\
&\quad + \cdots,
\end{aligned} \tag{22}$$

where

$$\begin{aligned}
\Phi_1^{[0]} &= \begin{pmatrix} \varphi_1^{[0]} \\ \phi_1^{[0]} \end{pmatrix}, \\
\Phi_1^{[1]} &= \begin{pmatrix} \varphi_1^{[1]} \\ \phi_1^{[1]} \end{pmatrix}, \\
\Phi_1^{[2]} &= \begin{pmatrix} \varphi_1^{[2]} \\ \phi_1^{[2]} \end{pmatrix}, \\
&\vdots,
\end{aligned} \tag{23}$$

and $(\varphi_1^{[i-1]}, \phi_1^{[i-1]})^{\mathrm{T}}$ $(i = 1, 2, 3)$ are given in Appendix A.

It is clearly observed that $\Phi_1^{[0]}$ is a solution of the Lax pair (4a) and (4b) at $q[0] = e^{it}$ and $\lambda = i$. Hence, substituting $\Phi_1^{[0]}$, $q[0] = e^{it}$, and $\lambda = i$ into (12), the first-order rogue wave solution of equation (2) is obtained

$$q[1] = \left(1 + 4\frac{G_1 + i4t}{H_1}\right)e^{it}, \tag{24}$$

where

$$H_1 = 2 + 80xt\varepsilon + 200t^2\varepsilon^2 + 8t^2 + 8x^2, \tag{25a}$$

$$G_1 = 1 - 40xt\varepsilon - 100t^2\varepsilon^2 - 4t^2 - 4x^2. \tag{25b}$$

There is only a free parameter ε in the first-order solution, which corresponds to the fifth-order nonlinear effects of (2). If different parameter values are taken, there are different

nonlinear phenomena in (2). The picture of the solution is depicted, as shown in Figure 1. Figure 1(a) displays change of the amplitude and Figure 1(b) is the density plot. In Figures 1(a) and 1(b), we have $\varepsilon = 0$. In Figures 1(c) and 1(d), there is $\varepsilon = 0.2$. Fixing $x = 0$, the changes of $|q[1](0,t)|$ in the direction of t axes with the parameters $\varepsilon = 0$ are displayed in Figure 1(e). It is observed from Figure 1(e) that the maximum amplitude of $|q[1](0,x)|$ is 3, which occurs at $t = 0$.

Then, considering the following limit

$$\begin{aligned}\lim_{\delta\to 0}\frac{\left[T_1[1]\big|_{\lambda=\lambda_1+\delta}\right]\Psi}{\delta} &= \lim_{\delta\to 0}\frac{\left[\delta + T_1[1]\big|_{\lambda=\lambda_1}\right]\Psi}{\delta} \\ &= \Phi_1^{[0]} + T_1[1](\lambda_1)\Phi_1^{[1]} = \Phi_1[1],\end{aligned} \tag{26a}$$

$$\Phi_1[1] = \begin{pmatrix}\varphi_1[1]\\ \phi_1[1]\end{pmatrix}, \tag{26b}$$

where $T_1[1]$ and $\Phi_1[1]$ can be calculated by Maple.

We neglect $\Phi_1[1]$ since its expression is rather cumbersome to write it down. Then, we obtain the second-order rogue wave solution of (2)

$$q[2] = q[1] + 4\frac{\varphi_1[1]\cdot\phi_1[1]^*}{|\varphi_1[1]|^2 + |\phi_1[1]|^2}, \tag{27}$$

where

$$\Delta = 1 + 40xt\varepsilon + 100t^2\varepsilon^2 + 4t^2 + 4x^2, \tag{28a}$$

$$\begin{aligned}\varphi_1[1] &= \frac{1}{3\Delta}e^{it/2}(A_1 + iB_1),\\ \phi_1[1] &= \frac{1}{3\Delta}e^{-it/2}(A_2 + iB_2),\end{aligned} \tag{28b}$$

and A_1, B_1, A_2, and B_2 are given in Appendix B.

In (27), there are three free parameters ε, a_1, and b_1. Different values will be taken to demonstrate different second-order nonlinear rogue waves. The corresponding graph of the rogue wave is displayed in Figure 2. In Figures 2(a) and 2(b), we have $\varepsilon = 0$ and $a_1 = b_1 = 0$. It is a basic form which reaches a single maximum at the center in Figure 2(a). Figure 2(b) looks like "Z" type. By slightly adjusting the parameter $\varepsilon = 0.2$ and other parameters being the same, the rogue waves are depicted, as displayed in Figures 2(c) and 2(d). In this case, two small peaks are located on both sides and the other two peaks are located near high peak. Nearly all power of the rogue wave is focused on the high peak. It is observed from Figure 2(a) that the maximum amplitude of $|q[1](0,x)|$ is 5, which occurs at $t = 0$.

Then, changing the parameters a_1 and b_1 in $\Omega(\delta)$ and letting $\varepsilon = 0$, the picture of the rogue waves is exhibited in Figure 3. In Figures 3(a) and 3(b), we have $a_1 = 10$ and $b_1 = 0$. In Figures 3(c) and 3(d), there are $a_1 = 0$ and $b_1 = 20$. In Figures 3(a)–3(d), the solution $q[2]$ splits into three first-order rogue waves, which are not separated completely. In Figures 3(a)–3(d), three first-order rogue waves have a structure of an equilateral triangle. Furthermore, it is found that the temporal-interval in which the rogue waves appear is enlarged. The solution $q[2]$ splits into three first-order rogue wave separated completely as the increase of a_1 and b_1. When $\varepsilon = 0.1$ and $a_1 = b_1 = 40$, the plot of the rogue waves is depicted in Figures 3(e) and 3(f). The numerical results indicate that the maximum amplitude of solution $q[2]$ varies with the change of the parameters ε, a_1, and b_1.

Likewise, we study the third-order solution $q[3]$ of (2). Considering the limitation below

$$\begin{aligned}\lim_{\delta\to 0}\frac{\left[\delta + T_1[2]\big|_{\lambda=\lambda_1}\right]\left[\delta + T_1[1]\big|_{\lambda=\lambda_1}\right]\Psi}{\delta^2} &= \Phi_1^{[0]} + \left(T_1[1](\lambda_1) + T_1[2](\lambda_1)\right)\Phi_1^{[1]}\\ &\quad + T_1[2](\lambda_1)T_1[1](\lambda_1)\Phi_1^{[2]} = \Phi_1[2],\end{aligned} \tag{29a}$$

$$\Phi_1[2] = \begin{pmatrix}\varphi_1[2]\\ \phi_1[2]\end{pmatrix}, \tag{29b}$$

where $T_1[2]$ and $\Phi_1[2]$ are calculated by the Maple.

We neglect $T_1[2]$ and $\Phi_1[2]$ since the expressions are too boring to write them down in the paper. Then, the third-order rogue wave solution of (2) is obtained

$$q[3] = q[2] + 4\frac{\varphi_1[2]\cdot\phi_1[2]^*}{|\varphi_1[2]|^2 + |\phi_1[2]|^2}. \tag{30}$$

There are five parameters $\varepsilon, a_1, b_1, a_2$, and b_2 in the solution $q[3]$. The corresponding pictures of $q[3]$ are described in Figure 4. In Figures 4(a) and 4(b), we have $\varepsilon = 0$, $a_1 = b_1 = 0$, and $a_2 = b_2 = 0$. It is a fundamental pattern and there is a single maximum at the center where the maximum amplitude of $q[3]$ is 7. Increasing the parameter $\varepsilon = 0.5$ while the other parameters are unchanged, the solution $q[3]$ is shown in Figures 4(c) and 4(d).

When we select the parameters as $\varepsilon = 0.02$ and $b_1 = 500$, the pictures of the solution $q[3]$ are illustrated in Figures 5(a) and 5(b). Changing the parameter ε as $\varepsilon = 0.25$, the corresponding plots of the solution $q[3]$ are depicted in Figures 6(a) and 6(b). Comparing with Figures 5 and 6, it is seen that the third-order rogue waves are composed of six first-order rogue waves and six waves form a triangle. However, it is found that six first-order rogue waves form an equilateral triangle in Figure 5(b) while the waves form an isosceles triangle in Figure 6(b).

When the parameters $\varepsilon = 0.02$ and $b_2 = 1500$, the plots of the solution $q[3]$ are demonstrated in Figure 7. It can be observed from Figure 7 that the shape is a pentagon, where one wave is located in the center, and the others are the vertices of the pentagon.

If the parameters $\varepsilon = 0.02$, $b_1 = 500$, and $b_2 = 10000$, the pictures of the solution $q[3]$ are illustrated in Figure 8. It is found that Figure 8(a) also consists of the six first-order rogue waves. Interestingly, one wave is on the left side and the other four waves form a rectangle, and the last lies in the center. It is known from Figure 8(b) that six first-order rogue waves form a triangle on the left side and a rectangle on the right side.

With the increase of the order for the rogue waves solutions $q[N]$, there are more free parameters, which will

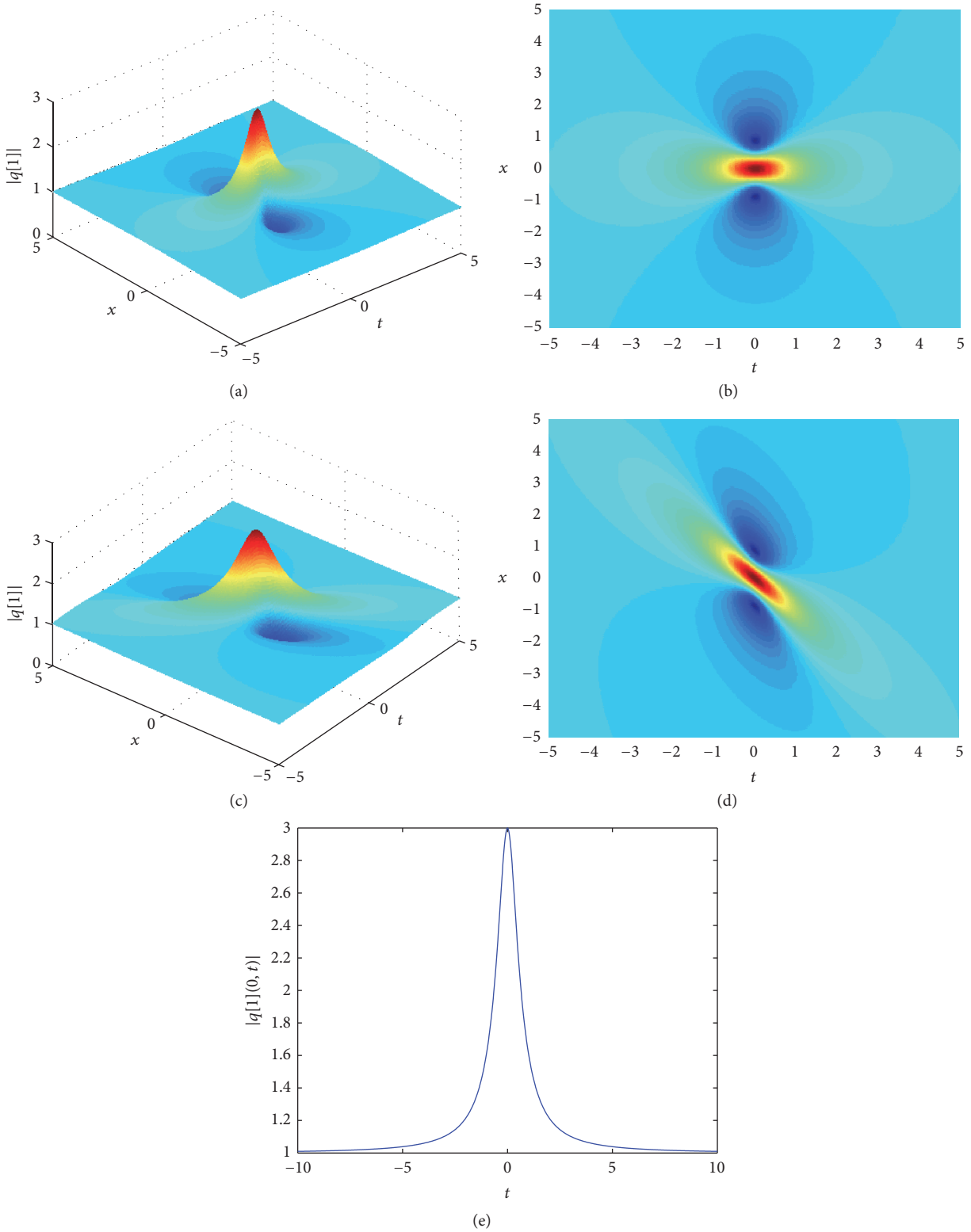

FIGURE 1: (a) The first-order rogue wave with $\varepsilon = 0$; (b) the density plot with $\varepsilon = 0$; (c) the first-order rogue wave with $\varepsilon = 0.2$; (d) the density plot with $\varepsilon = 0.2$; (e) the section of $|q[1](0, t)|$ at $x = 0$ with $\varepsilon = 0$.

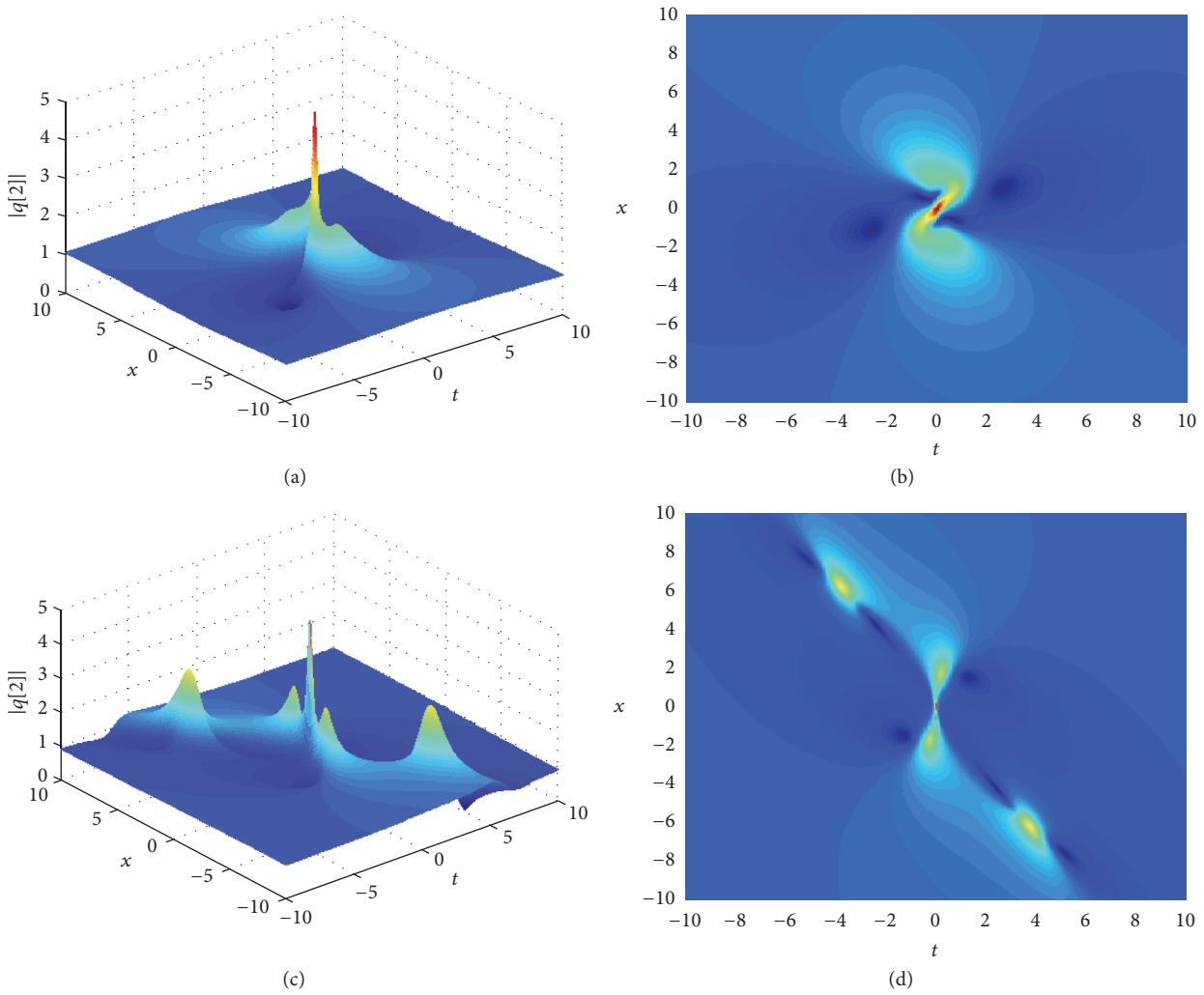

Figure 2: (a) The second-order rogue wave with $\varepsilon = 0$ and $a_1 = b_1 = 0$; (b) the density plot with $\varepsilon = 0$ and $a_1 = b_1 = 0$; (c) the second-order rogue wave with $\varepsilon = 0.2$ and $a_1 = b_1 = 0$; (d) the density plot with $\varepsilon = 0.2$ and $a_1 = b_1 = 0$.

exhibit more novel and interesting structures. It is supposed that the new structures of the higher-order rogue waves will be polygon of different shape.

4. Conclusions

In the paper, the Nth-order solutions of the rogue waves are constructed by using the generalized Darboux transformation (DT) for the inhomogeneous fifth-order nonlinear Schrödinger equation. Firstly, a short introduction about the DT is given. Secondly, the generalized DT is discussed making use of the Taylor expansion and a limit procedure. The first-, second-, and third-order rogue waves solutions are derived. Changing the free parameters in the solutions, some new structures of the rogue waves are obtained. By analyzing the nonlinear dynamics of the rogue waves, we can study the rogue waves in optical fibers. Furthermore, if the iteration process of the generalized DT is carried out continually, there will be more complicated and interesting structures of the rogue waves. It is hoped that the theoretical results will be confirmed by experiments in the future.

Appendix

A. Elements Expression

Analytical expressions of the coefficients in (21a), (21b), and (21c) are given as

$$\varphi_1^{[0]} = e^{it/2}\left(2x + 10t\varepsilon + 2it + 1\right),$$

$$\phi_1^{[0]} = e^{-it/2}\left(-2x - 10t\varepsilon - 2it + 1\right),$$

$$\varphi_1^{[1]} = e^{it/2}\left(-t^2 + \frac{250}{3}t^3\varepsilon^3 + 2a_1 - \frac{1}{4} + 25t^2\varepsilon^2 - 10t^3\varepsilon + 2ib_1 + \frac{325}{2}t\varepsilon + \frac{5}{2}it + 10it^2\varepsilon + 50it^3\varepsilon^2 - \frac{2}{3}it^3 - 2t^2x + 50t^2\varepsilon^2x + \frac{1}{2}x + 20it^2\varepsilon x + 10t\varepsilon x\right.$$

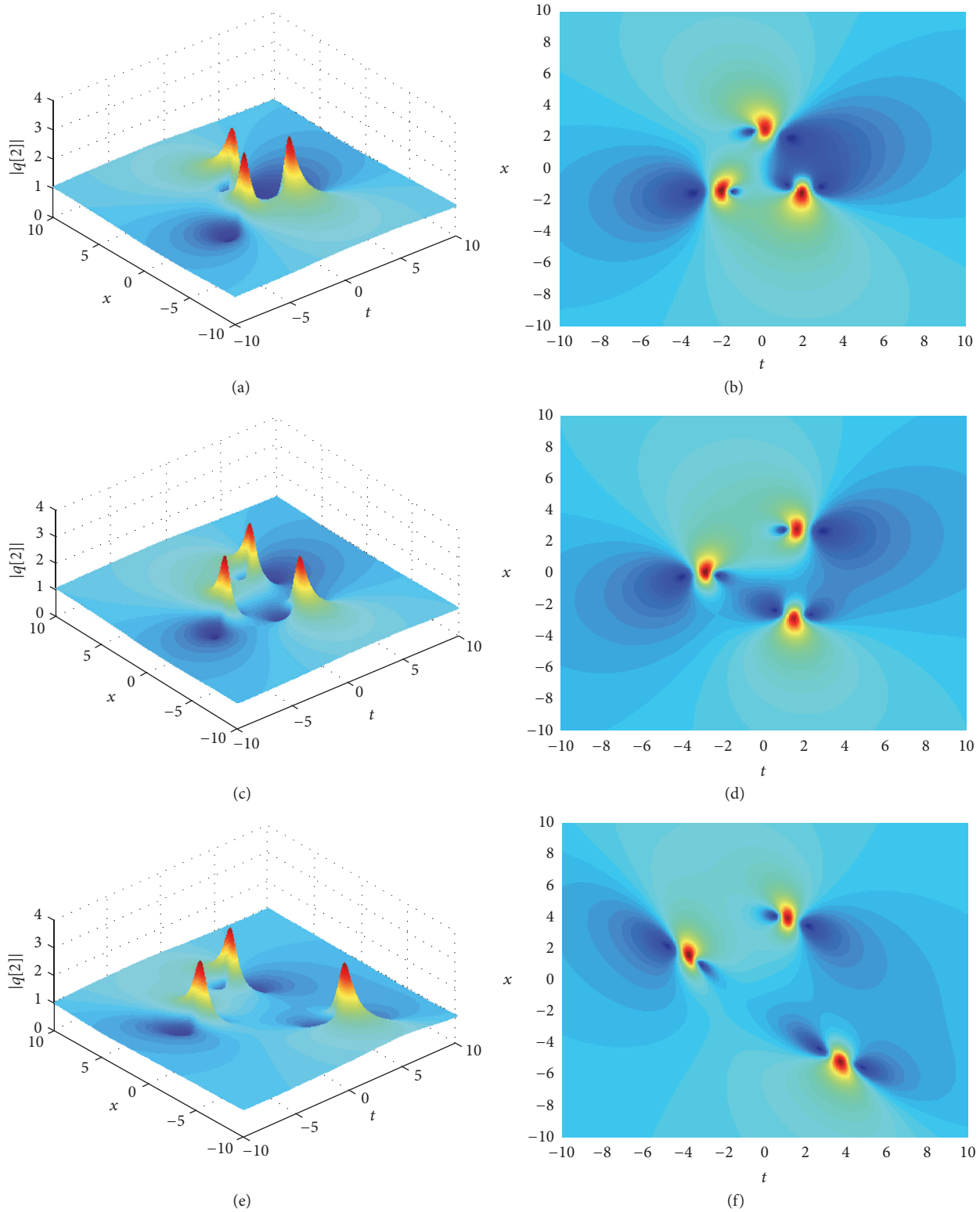

FIGURE 3: (a) The second-order rogue wave with $\varepsilon = 0$, $a_1 = 10$, and $b_1 = 0$; (b) the density plot with $\varepsilon = 0$, $a_1 = 10$, and $b_1 = 0$; (c) the second-order rogue wave with $\varepsilon = 0$, $a_1 = 0$, and $b_1 = 20$; (d) the density plot with $\varepsilon = 0$, $a_1 = 0$, and $b_1 = 20$; (e) the second-order rogue wave with $\varepsilon = 0.1$ and $a_1 = b_1 = 40$; (f) the density plot with $\varepsilon = 0.1$ and $a_1 = b_1 = 40$.

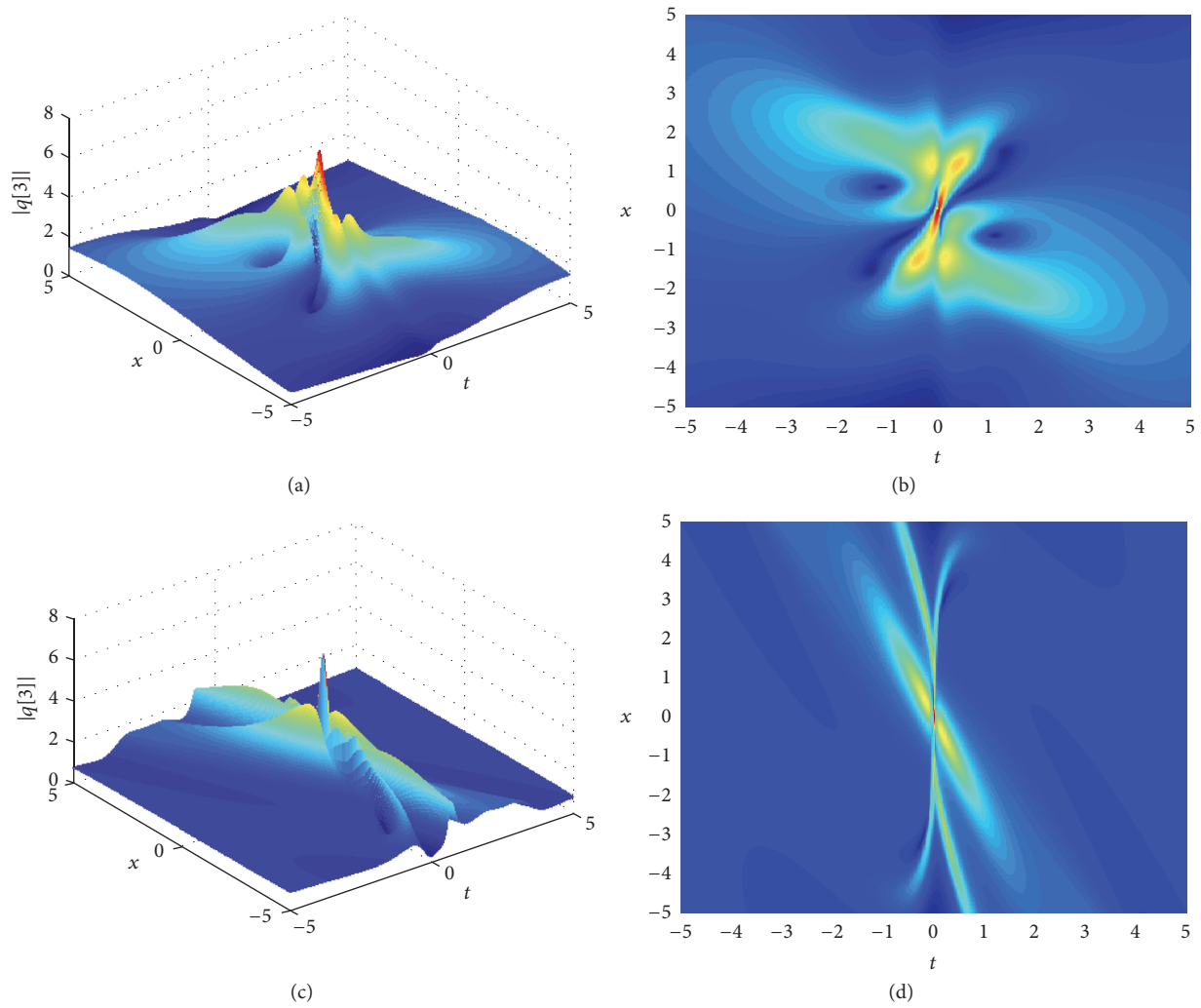

FIGURE 4: (a) The third-order rogue wave with $\varepsilon = 0$, $a_1 = b_1 = 0$, and $a_2 = b_2 = 0$; (b) the density plot with $\varepsilon = 0$, $a_1 = b_1 = 0$, and $a_2 = b_2 = 0$; (c) the third-order rogue wave with $\varepsilon = 0.5$, $a_1 = b_1 = 0$, and $a_2 = b_2 = 0$; (d) the density plot with $\varepsilon = 0.5$, $a_1 = b_1 = 0$, and $a_2 = b_2 = 0$.

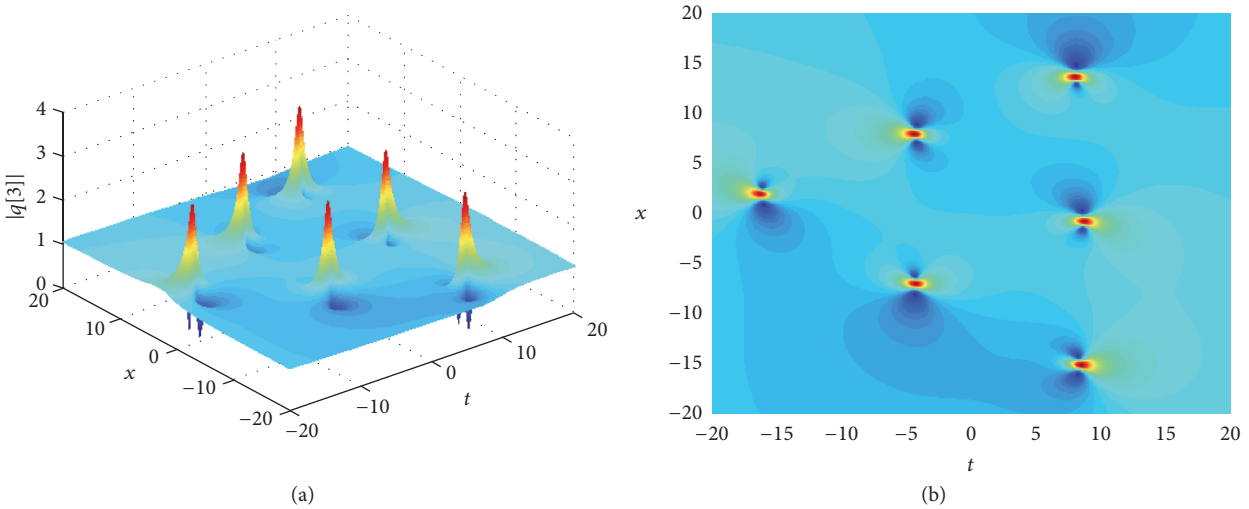

FIGURE 5: (a) The third-order rogue wave with $\varepsilon = 0.02$ and $b_1 = 500$; (b) the density plot with $\varepsilon = 0.02$ and $b_1 = 500$.

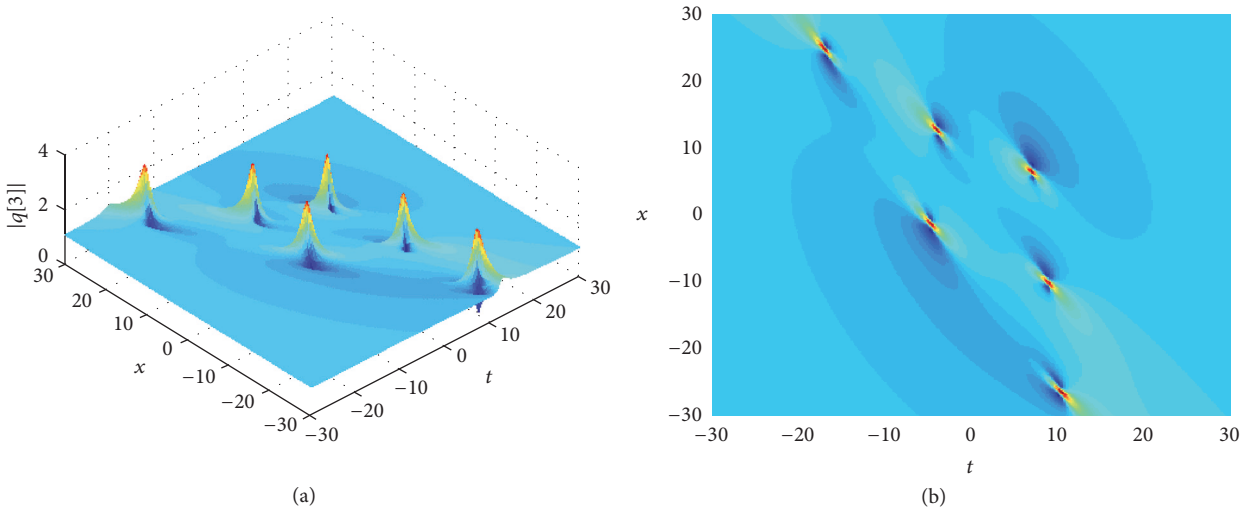

FIGURE 6: (a) The third-order rogue wave with $\varepsilon = 0.25$ and $b_1 = 500$; (b) the density plot with $\varepsilon = 0.25$ and $b_1 = 500$.

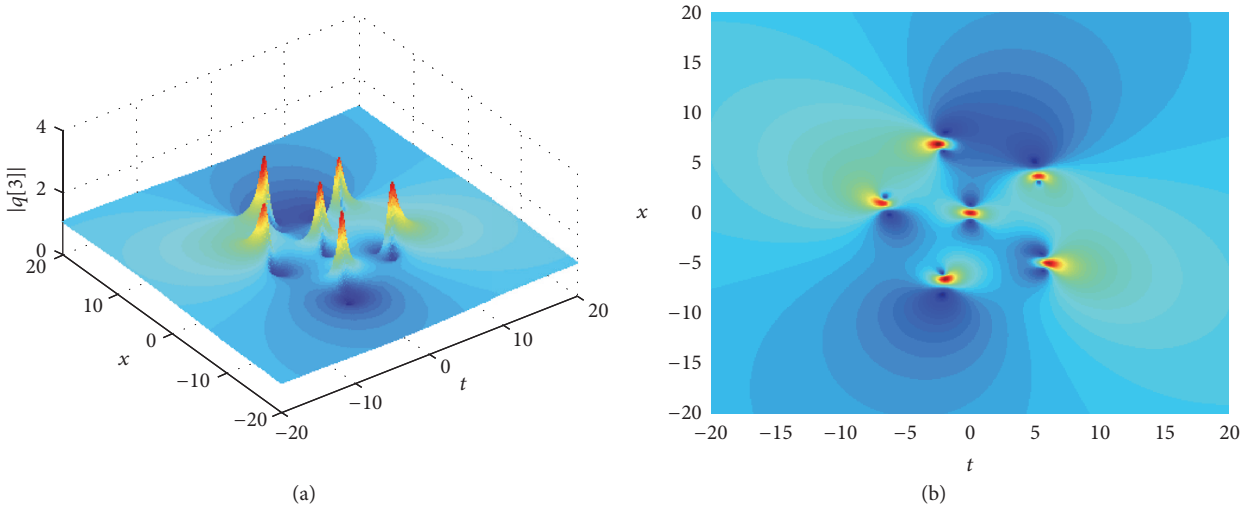

FIGURE 7: (a) The third-order rogue wave with $\varepsilon = 0.02$ and $b_2 = 1500$; (b) the density plot with $\varepsilon = 0.02$ and $b_2 = 1500$.

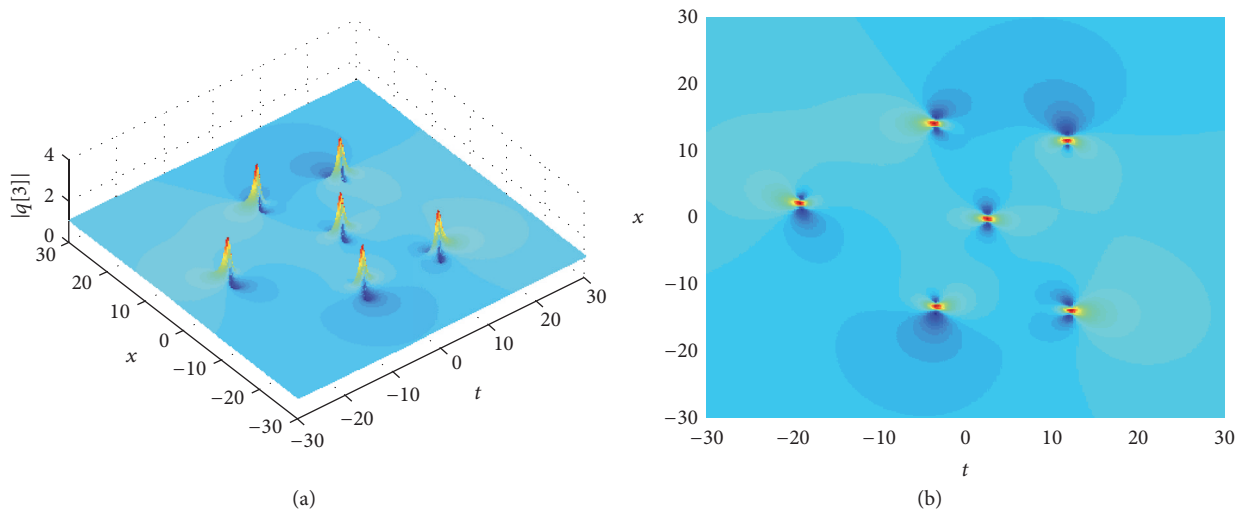

FIGURE 8: (a) The third-order rogue wave with $\varepsilon = 0.02$, $b_1 = 500$, and $b_2 = 10000$; (b) the density plot with $\varepsilon = 0.02$, $b_1 = 500$, and $b_2 = 10000$.

$$+ 2itx + 10t\varepsilon x^2 + 2itx^2 + x^2 + \frac{2}{3}x^3\Big),$$

$$\phi_1^{[1]} = e^{-it/2}\Big(-t^2 - \frac{250}{3}t^3\varepsilon^3 - 2a_1 - \frac{1}{4} + 25t^2\varepsilon^2 + 10t^3\varepsilon - 2ib_1 - \frac{325}{2}t\varepsilon - \frac{5}{2}it + 10it^2\varepsilon - 50it^3\varepsilon^2 + \frac{2}{3}it^3 + 2t^2x - 50t^2\varepsilon^2x - \frac{1}{2}x - 20it^2\varepsilon x + 10t\varepsilon x + 2itx - 10t\varepsilon x - 2itx^2 + x^2 - \frac{2}{3}x^3\Big),$$

$$\varphi_1^{[2]} = e^{it/2}\Big[\Big(\frac{5}{3}\varepsilon - \frac{250}{3}\varepsilon^3 + \frac{625}{3}\varepsilon^5\Big)t^5 + \Big(\frac{625}{6}\varepsilon^4 + \frac{1}{6} - 25\varepsilon^2{}_0\Big)t^4 + \Big(-\frac{375}{2}\varepsilon + \frac{8125}{2}\varepsilon^3\Big)t^3\Big(-2a_1 + 50\varepsilon^2a_1 + \frac{3225}{4}\varepsilon^2 - 20\varepsilon b_1 - \frac{9}{4}\Big)t^2 + \Big(10\varepsilon a_1 - 2b_1 + \frac{3963}{16}\varepsilon\Big)t + \Big(\frac{1}{6} + \frac{5}{3}\varepsilon t\Big)x^4 + \Big(\Big(\frac{50}{3}\varepsilon^2 - \frac{2}{3}\Big)t^2 + \frac{10}{3}\varepsilon t + \frac{1}{2}\Big)x^3 + \Big(\Big(-10\varepsilon + \frac{250}{3}\varepsilon^3\Big)t^3 + \big(25\varepsilon^2 - 1\big)t^2 + \frac{335}{2}\varepsilon t - \frac{1}{4} + 2a_1\Big)x^2 + \Big(\Big(\frac{1}{3} - 50\varepsilon^2 + \frac{625}{3}\varepsilon^4\Big)t^4 + \Big(\frac{250}{3}\varepsilon^3 - 10\varepsilon\Big)t^3 + \Big(\frac{3275}{2}\varepsilon^2 - \frac{11}{2}\Big)t^2 + \Big(20\varepsilon a_1 + \frac{325}{2}\varepsilon - 4b_1\Big)t - \frac{1}{16} + 2a_1\Big)x + \frac{1}{2}a_1 + \frac{3}{32} + 2a_2 + \frac{1}{15}x^5 + i\Big(\frac{1}{3}tx^4 + \Big(\frac{20}{3}\varepsilon t^2 + \frac{2}{3}\Big)t\Big) \cdot x^3 + \Big(\Big(-50\varepsilon^2 - \frac{2}{3}\Big)t^3 + 10\varepsilon t^2 + \Big(\frac{7}{2}t + 2b_1\Big)\Big)x^2 + \Big(\Big(\frac{500}{3}\varepsilon^3 - \frac{20}{3}\varepsilon\Big)t^4 + \Big(50\varepsilon^2 - \frac{2}{3}\Big)t^3 + 355\varepsilon t^2 + \Big(20\varepsilon b_1 + 4a_1 + \frac{5}{2}\Big)t + 2bx_1 + \Big(\frac{625}{3}\varepsilon^4 - \frac{50}{3}\varepsilon^2 + \frac{1}{15}\Big)t^5 + \Big(-\frac{10}{3}\varepsilon + \frac{250}{3}\varepsilon^3\Big)t^4 + \Big(\frac{3375}{2}\varepsilon^2 - \frac{5}{2}\Big)t^3 + \Big(20\varepsilon a_1 + \frac{345}{2}\varepsilon + 50\varepsilon^2b_1 - 2b_1\Big)t^2 + \Big(\frac{7}{16} + 10\varepsilon b_1 + 2a_1\Big)t + 2b_2\Big)\Big],$$

$$\phi_1^{[2]} = e^{-it/2}\Big[\Big(-\frac{5}{3}\varepsilon + \frac{250}{3}\varepsilon^3 - \frac{625}{3}\varepsilon^5\Big)t^5 + \Big(\frac{625}{6}\varepsilon^4 - 25\varepsilon^2\Big)t^4 + \Big(\frac{375}{2}\varepsilon - \frac{8125}{2}\varepsilon^3\Big)t^3 + \Big(2a_1 - 50\varepsilon^2a_1 + \frac{3225}{4}\varepsilon^2 + 20\varepsilon b_1 - \frac{9}{4}\Big)t^2 + \Big(10\varepsilon a_1 - 2b_1 - \frac{3963}{16}\varepsilon\Big)t + \Big(\frac{1}{6} - \frac{5}{3}\varepsilon t\Big)x^4 + \Big(\Big(-\frac{50}{3}\varepsilon^2 + \frac{2}{3}\Big)t^2 + \frac{10}{3}\varepsilon t - \frac{1}{2}\Big)x^3 + \Big(\Big(10\varepsilon - \frac{250}{3}\varepsilon^3\Big)t^3 + \big(25\varepsilon^2 - 1\big)t^2 - \frac{335}{2}\varepsilon t + \frac{1}{4} - 2a_1\Big)x^2 + \Big(\Big(-\frac{1}{3} + 50\varepsilon^2 + \frac{625}{3}\varepsilon^4\Big)t^4 + \Big(\frac{250}{3}\varepsilon^3 - 10\varepsilon\Big)t^3 + \Big(\frac{3275}{2}\varepsilon^2 - \frac{11}{2}\Big)t^2 + \Big(-20\varepsilon a_1 + \frac{325}{2}\varepsilon + 4b_1\Big)t + \frac{1}{16} + 2a_1\Big)x - \frac{1}{2}a_1 + \frac{3}{32} - 2a_2 - \frac{1}{15}x^5 + i\Big(-\frac{1}{3}tx^4 + \Big(-\frac{20}{3}\varepsilon t^2 + \frac{2}{3}t\Big)\Big)x^3 + \Big(\Big(-50\varepsilon^2 + \frac{2}{3}\Big)t^3 + 10\varepsilon t^2 + \Big(-\frac{7}{2}t - 2b_1\Big)\Big)x^2 + \Big(\Big(-\frac{500}{3}\varepsilon^3 + \frac{20}{3}\varepsilon\Big)t^4 + \Big(50\varepsilon^2 - \frac{2}{3}\Big)t^3 - 355\varepsilon t^2 + \Big(-20\varepsilon b_1 - 4a_1 + \frac{5}{2}\Big)t + 2b_1x\Big) + \Big(-\frac{625}{3}\varepsilon^4 + \frac{50}{3}\varepsilon^2 - \frac{1}{15}\Big)t^5 + \Big(-\frac{10}{3}\varepsilon + \frac{250}{3}\varepsilon^3\Big)t^4 + \Big(-\frac{3375}{2}\varepsilon^2 + \frac{5}{2}\Big)t^3 + \Big(-20\varepsilon a_1 + \frac{345}{2}\varepsilon - 50\varepsilon^2b_1 + 2b_1\Big)t^2 + \Big(-\frac{7}{16} + 10\varepsilon b_1 + 2a_1\Big)t - 2b_2\Big]. \tag{A.1}$$

B. Coefficients

Analytical expressions of the coefficients in (26a) and (26b) are given as

$$A_1 = (-32t + 24)x^3 + \big(-480\varepsilon t^2 + (24 + 360\varepsilon)t + 12\big)x^2 + \big(\big(-2400\varepsilon^2 - 32\big)t^3 + \big(24 + 240\varepsilon + 1800\varepsilon^2\big)t^2 + (24 + 120\varepsilon)t + 6 + 24b_1\big)x + \big(-160\varepsilon - 4000\varepsilon^3\big)t^4 + \big(600\varepsilon^2 - 8 + 120\varepsilon\big)t^3 + \big(12 + 300\varepsilon^2 - 1800\varepsilon + 3000\varepsilon^3\big)t^2 + \big(120\varepsilon b_1 + 30\varepsilon - 24a_1 - 18\big)t + 3 - 12b_1,$$

$$
\begin{aligned}
B_1 &= 16x^4 + (-8 + 320\varepsilon t)\, x^3 + \left(2400\varepsilon^2 t^2 \right. \\
&\quad \left. + (24 - 120\varepsilon)\, t - 12\right) x^2 + \left(8000\varepsilon^3 t^3 \right. \\
&\quad \left. + \left(24 + 240\varepsilon - 600\varepsilon^2\right) t^2 - 2040\varepsilon t + 6 - 24a_1\right) x \\
&\quad + \left(10000\varepsilon^4 - 16\right) t^4 + \left(-1000\varepsilon^3 + 24 + 120\varepsilon \right. \\
&\quad \left. + 600\varepsilon^2\right) t + \left(-36 - 9900\varepsilon^2\right) t^2 + (990\varepsilon - 24b_1 + 6 \\
&\quad - 120\varepsilon a_1)\, t + 12a_1, \\
A_2 &= (-32t - 24)\, x^3 + \left(-480\varepsilon t^2 + (-24 - 360\varepsilon)\, t \right. \\
&\quad \left. + 12\right) x^2 + \left(\left(-2400\varepsilon^2 - 32\right) t^3 \right. \\
&\quad \left. + \left(-24 - 240\varepsilon - 1800\varepsilon^2\right) t^2 + (24 + 120\varepsilon)\, t - 6 \right. \\
&\quad \left. + 24b_1\right) x + \left(-160\varepsilon - 4000\varepsilon^3\right) t^4 + \left(-600\varepsilon^2 + 8 \right. \\
&\quad \left. - 120\varepsilon\right) t^3 + \left(12 + 300\varepsilon^2 - 1800\varepsilon - 3000\varepsilon^3\right) t^2 \\
&\quad + (120\varepsilon b_1 - 30\varepsilon - 24a_1 + 18)\, t + 3 + 12b_1, \\
B_2 &= 16x^4 + (8 + 320\varepsilon t)\, x^3 + \left(2400\varepsilon^2 t^2 \right. \\
&\quad \left. + (-24 + 120\varepsilon)\, t - 12\right) x^2 \\
&\quad + \left(\left(8000\varepsilon^3 t^3 + \left(600\varepsilon^2 - 24 - 240\varepsilon\right) t^2 - 2040\varepsilon\right) t \right. \\
&\quad \left. - 6 - 24a_1\right) x + \left(10000\varepsilon^4 - 16\right) t^4 + \left(1000\varepsilon^3 - 24 \right. \\
&\quad \left. - 120\varepsilon - 600\varepsilon^2\right) t + \left(-36 - 9900\varepsilon^2\right) t^2 + (-990\varepsilon \\
&\quad - 24b_1 - 6 - 120\varepsilon a_1)\, t - 12a_1.
\end{aligned}
\tag{B.1}
$$

Conflicts of Interest

The authors declare that they have no conflicts of interest.

Acknowledgments

The authors gratefully acknowledge the support of the National Natural Science Foundation of China (NNSFC) through Grant no. 11602232 and the National Sciences Foundation of Shanxi Province through Grant no. 2015011009.

References

[1] L. Draper, "Freak ocean waves," *Marine Observer*, vol. 35, pp. 193–195, 1965.

[2] A. R. Osborne, *Nonlinear Ocean Waves*, Academic Press, 2009.

[3] C. Kharif and E. Pelinovsky, "Physical mechanisms of the rogue wave phenomenon," *European Journal of Mechanics. B. Fluids*, vol. 22, no. 6, pp. 603–634, 2003.

[4] M. Onorato, A. R. Osborne, M. Serio, and L. Cavaleri, "Modulational instability and non-Gaussian statistics in experimental random water-wave trains," *Physics of Fluids*, vol. 17, no. 7, pp. 1–4, 2005.

[5] D. R. Solli, C. Ropers, P. Koonath, and B. Jalali, "Optical rogue waves," *Nature*, vol. 450, no. 7172, pp. 1054–1057, 2007.

[6] D.-I. Yeom and B. J. Eggleton, "Photonics: Rogue waves surface in light," *Nature*, vol. 450, no. 7172, pp. 953-954, 2007.

[7] J. M. Dudley, G. Genty, F. Dias, B. Kibler, and N. Akhmediev, "Modulation instability, Akhmediev Breathers and continuous wave supercontinuum generation," *Optics Express*, vol. 17, no. 24, pp. 21497–21508, 2009.

[8] Y. V. Bludov, V. V. Konotop, and N. Akhmediev, "Matter rogue waves," *Physical Review A*, vol. 80, no. 3, Article ID 033610, 2009.

[9] A. N. Ganshin, V. B. Efimov, G. V. Kolmakov, L. P. Mezhov-Deglin, and P. V. E. McClintock, "Observation of an inverse energy cascade in developed acoustic turbulence in superfluid helium," *Physical Review Letters*, vol. 101, no. 6, Article ID 065303, 2008.

[10] M. S. Ruderman, "Freak waves in laboratory and space plasmas," *European Physical Journal: Special Topics*, vol. 185, no. 1, pp. 57–66, 2010.

[11] L. Stenflo and M. Marklund, "Rogue waves in the atmosphere," *Journal of Plasma Physics*, vol. 76, no. 3-4, pp. 293–295, 2010.

[12] Z.-Y. Yan, "Financial rogue waves," *Communications in Theoretical Physics*, vol. 54, no. 5, pp. 947–949, 2010.

[13] V. Ruban, Y. Kodama, M. Ruderman et al., "Rogue waves - towards a unifying concept?: Discussions and debates," *European Physical Journal: Special Topics*, vol. 185, no. 1, pp. 5–15, 2010.

[14] D. H. Peregrine, "Water waves, nonlinear Schrödinger equations and their solutions," *Australian Mathematical Society Journal B: Applied Mathematics*, vol. 25, no. 1, pp. 16–43, 1983.

[15] N. Akhmediev, A. Ankiewicz, and J. M. Soto-Crespo, "Rogue waves and rational solutions of the nonlinear Schrödinger equation," *Physical Review E - Statistical, Nonlinear, and Soft Matter Physics*, vol. 80, no. 2, Article ID 026601, 2009.

[16] V. B. Matveev and M. A. Salle, *Darboux Transformations and Solitons*, Springer, Berlin, Gemany, 1991.

[17] B. Guo, L. Ling, and Q. P. Liu, "Nonlinear schrödinger equation: generalized darboux transformation and rogue wave solutions," *Physical Review E*, vol. 85, no. 2, Article ID 026607, 2012.

[18] Zhaqilao, "On Nth-order rogue wave solution to the generalized nonlinear Schrödinger equation," *Physics Letters. A*, vol. 377, no. 12, pp. 855–859, 2013.

[19] N. Song, W. Zhang, and M. H. Yao, "Complex Nonlinearities of Rogue Waves in Generalized Inhomogeneous Higher-Order Nonlinear Schrödinger Equation," *Nonlinear Dynamics*, vol. 82, no. 1-2, pp. 489–500, 2015.

[20] X. Lv and F. Lin, "Soliton excitations and shape-changing collisions in alpha helical proteins with interspine coupling at higher order," *Communications in Nonlinear Science and Numerical Simulation*, vol. 32, pp. 241–261, 2016.

[21] X. Lv and W.-X. Ma, "Study of lump dynamics based on a dimensionally reduced Hirota bilinear equation," *Nonlinear Dynamics*, vol. 85, no. 2, pp. 1217–1222, 2016.

[22] G. Huang, Z.-P. Shi, X. Dai, and R. Tao, "Soliton excitations in the alternating ferromagnetic Heisenberg chain," *Physical Review B*, vol. 43, no. 13, pp. 11197–11206, 1991.

[23] M. Daniel and L. Kavitha, "Localized spin excitations in an anisotropic Heisenberg ferromagnet with Dzyaloshinskii-Moriya interactions," *Physical Review B*, vol. 63, no. 17, 2001.

[24] J. Lamb, "Solitons and the motion of helical curves," *Physical Review Letters*, vol. 37, no. 5, pp. 235–237, 1976.

[25] L. Kavitha and M. Daniel, "Integrability and soliton in a classical one-dimensional site-dependent biquadratic Heisenberg spin chain and the effect of nonlinear inhomogeneity," *Journal of Physics. A. Mathematical and General*, vol. 36, no. 42, pp. 10471–10492, 2003.

[26] M. Wang, W.-R. Shan, B. Tian, and Z. Tan, "Darboux transformation and conservation laws for an inhomogeneous fifth-order nonlinear Schrödinger equation from the Heisenberg ferromagnetism," *Communications in Nonlinear Science and Numerical Simulation*, vol. 20, no. 3, pp. 692–698, 2015.

[27] R. Radha and V. R. Kumar, "Explode-Decay Solitons in the Generalized Inhomogeneous Higher-Order Nonlinear Schrödinger Equations," *Zeitschrift für Naturforschung A*, vol. 62, no. 7-8, 2007.

[28] W.-Z. Zhao, Y.-Q. Bai, and K. Wu, "Generalized inhomogeneous Heisenberg ferromagnet model and generalized nonlinear Schrödinger equation," *Physics Letters. A*, vol. 352, no. 1-2, pp. 64–68, 2006.

[29] X. Lv, W.-X. Ma, J. Yu, and C. . Khalique, "Solitary waves with the Madelung fluid description: A generalized derivative nonlinear Schrödinger equation," *Communications in Nonlinear Science and Numerical Simulation*, vol. 31, no. 1-3, pp. 40–46, 2016.

[30] D.-S. Wang, S. Yin, Y. Tian, and Y. Liu, "Integrablility and bright soliton solutions to the coupled nonlinear Schrödinger equation with higher-order effects," *Applied Mathematics and Computation*, vol. 229, pp. 296–309, 2014.

[31] X. Lv, F. Lin, and F. Qi, "Analytical study on a two-dimensional Korteweg-de Vries model with bilinear representation, Backlund transformation and soliton solutions," *Applied Mathematical Modelling*, vol. 39, no. 12, pp. 3221–3226, 2015.

[32] D.-S. Wang, D.-J. Zhang, and J. Yang, "Integrable properties of the general coupled nonlinear Schrödinger equation," *Journal of Mathematical Physics*, vol. 51, no. 2, Article ID 023510, 17 pages, 2010.

[33] U. Al Khawaja, "A comparative analysis of Painlevé, Lax pair, and similarity transformation methods in obtaining the integrability conditions of nonlinear Schrödinger equations," *Journal of Mathematical Physics*, vol. 51, no. 5, Article ID 053506, 11 pages, 2010.

[34] D.-S. Wang and X. Wei, "Integrability and exact solutions of a two-component Korteweg–de Vries system," *Applied Mathematics Letters. An International Journal of Rapid Publication*, vol. 51, pp. 60–67, 2016.

[35] X. Lv, W.-X. Ma, S.-T. Chen, and C. M. Khalique, "A note on rational solutions to a Hirota-Satsuma-like equation," *Applied Mathematics Letters*, vol. 58, pp. 13–18, 2016.